

Powder feeding in a powder engine under different gas-solid ratios



Chao Li ^{a,*}, Xiaofei Zhu ^b, Zhe Deng ^c, Jiangang Yang ^d, Chunbo Hu ^d, Jinjia Wei ^a

^a School of Chemical Engineering and Technology, Xi'an Jiaotong University, Xi'an, 710049, PR China

^b Aerospace System Engineering Shanghai, Shanghai, 201109, China

^c Modern Chemistry Research Institute, Xi'an, 710065, PR China

^d Science and Technology on Combustion, Internal Flow and Thermo-Structure Laboratory, Northwestern Polytechnical University, Xi'an, Shaanxi, 710072, PR China

ARTICLE INFO

Keywords:

Powdered engine
 Solid-gas two-phase flow
 Powder feeding
 Mass flow rate
 Gas-solid ratio

ABSTRACT

It is a key and difficult problem to find the optimal powder-feeding technique in the study of powdered engines. In this paper, the feeding of powder in powder engines at different gas-solid ratios was experimentally investigated. Working characteristics of the classic piston-driven powder feeding system were obtained. A high linear tendency between powder mass flow rate and the minimum throttle channel area is observed from the experiment. The solid-gas mass ratio to maintain a stable powder feeding is approximately valued in range of 34.4–54.6 under different throttle channel areas. The least deviation in the relative powder mass flow rate for the tests is –15% to +8%. Due to the high uncertainty of the gas-solid flow structures at different gas-solid ratios, obvious low-frequency oscillations and high-frequency oscillations exist during the powder feeding process. The frequencies of low-frequency oscillations are mainly 1–3 Hz, while those of high-frequency oscillations are 20–30 Hz and 30–45 Hz in different tests.

1. Introduction

As advanced weapons and deep-space exploration technology continue to develop, demand for improved propulsion systems is growing. Due to the obvious advantages of thrust regulation, multiple-pulse ignition, high impulse, security, simple structure, and low cost [1], the new types powder engines have become a research hotspot. To date, the typical kinds of powder engines that have been studied are the Al/AP bipropellant powder rockets [1,2], powdered fuel ramjets [3], powdered fuel water ramjets [4], and Mg/CO₂ bipropellant powder rockets [5–7]. Their reliable operation and multiple pulse functions [2], as well as thrust regulation ignition functions [6], are all based on accurate and stable powder feeding. Thus, improving powder feeding technique is a key and difficult problem to be solved for powdered engines [8].

Due to its continuous powder-handling ability and the high gas and solid throughput, fluidization technology is one of the most important and widely used powder feeding technologies in industry [9]. However, this technology, as used in powdered engines, is more complex than that in industry or the natural environment. This is largely because of the higher requirements for powder-feeding processes and powder-feeding systems. The most important requirement is to achieve accurate

control of the powder mass flow rate and to achieve the miniaturization and integration of powder feeding system at the same time. Following this principle, the first powder-supply device for a powder engine was put forward in 1970 [10]. This is essentially a kind of piston-driven type powder-supply system. This idea also guided later work, which made improvements to powder-supply systems [1,11–14]. These powder supply systems can be divided into two categories according to the fluidization method, one is the fluidized bed method, the fluidization gas is introduced from the back end of the piston, the other is using high shear concentric air flow (“air knife”) to disperse powder, the gas is introduced from the location near the outlet of the powder storage tank.

The representative and typical fluidized bed powder supply method for powder rocket was proposed by Fricke in powder rocket feasibility evaluation [10]. By referring this idea, the complex fluidized bed powder supply system was improved into Positive Displacement Fluidized Bed (PDFB) supply system by Foote [15]. Meyer improved [16] fluidized bed type powder supply system for the aluminum/magnesium powder rocket, a linear displacement sensor was installed in the piston of the powder supply system to measure the velocity of the piston and calculate the mass flow rate of the powder. Subsequently, Miller [17] added a supplementary air channel at the outlet of the powder storage tank to balance the pressure in the storage tank and improve the stability of the

* Corresponding author.

E-mail address: lichao1990@live.cn (C. Li).

powder feeding system for long time operation. In addition, during the investigation of combustion of dispersions of metal powders, the smaller size powder feeding devices were used to provide micro powder flow rates. Malinin [18] proposed a micro powder feeding device in the investigation of combustion of aluminum-air suspensions, the device consists of a piston with a gas-permeable valve, and a locking and regulating valve with a drive. Similarly, during the study of combustion of boron particles cloud, Yagodnikov [19] optimized the piston, which has a hole through which the transporting gas is passed. Tizilov [20] also used fluidized bed method in his study on flame propagation in aluminum-air mixture flow.

When it comes to high shear concentric air flow method, the typical device was proposed by Goroshin [21,22], there is an annular air intake at the convergence section of the storage tank. The fluidization gas entering from the annular air intake could carry the particles out, and then flow through the convergence channel to enhance gas-solid mixing and improve the flow velocity. Similar method was also adopted in Risha's research [23]. Northwestern Polytechnical University was also committed to the development of powder supply system, and a more efficient powder supply system was designed [3,6]. Compared with Goroshin's design, the biggest difference is that the circular slit intake of fluidized gas is improved into an annular gas collecting cavity. This is because when the powder supply device is horizontally placed, the lower part of the circular slit is easy blocked by powder under the influence of gravity. In contrast, the air flow in the annular gas collecting cavity can form a shear air flow in the same direction as the powder movement, and the shear air velocity is high. Particles are quickly taken out of the storage tank under the action of tangential air flow, and it is not easy to deposit and block the air inlet hole.

Essentially, the working principles for these powder-supply devices are similar, incorporating a piston actuation and a gas fluidization method. Here, the fluidization gas is fed into a powder storage box to fluidize the powder and to make it to flow out. The piston is used to push the powder to fill the cavity left by the output powder. As the powder is pushed and fluidized, the fixed bed is gradually transformed into a fluidized bed, and the feeding process is completed through pipeline transportation. Using this method, a continuous powder feeding process is achieved [14].

To further optimize powder-feeding systems for powdered engines, Sun [14] experimentally investigated different powder mass flow-rate measurement methods and powder-feeding processes at high pressure. The powder-feeding process used in his experiment showed an obvious instability, and he pointed out that the emphasis should be on ensuring that the storage box pressure is steady. Yang [24] studied the starting and flow regulation characteristics of powder feeding for powder engines in choked and non-choked mode. The choked mode showed better flow-regulation performance. Other studies on powder-feeding systems for powdered engines mainly focus on the characteristics of pneumatic powder filling [25], the powder-filling ratio, and the fluidization performance of powder [26]. Studies of two-phase flow have largely focused on pickup characteristics during particle entrainment [27–32]. However, little investigation has been done on the macroscopic operating characteristics of a piston-driven powder-feeding system, such as on its stability and pressure oscillation characteristics. The operating characteristics are largely influenced by two-phase flow parameters and the structure features of a powder-feeding system. Therefore, studies on the ways that these factors affect the powder-feeding process can help obtain the operating characteristics of the system and provide experimental data to improve designs of the system.

In this paper, using a classic piston-driven powder-feeding system, an experimental system for powder feeding is established. The operating characteristics of the system at different solid-gas mass ratios are obtained, and analyses of the mass flow rate and pressure-oscillation characteristics are conducted.

2. Experimental specifications

2.1. Sample selection and experimental system

To universalize the research results of this paper, an experimental sample consistent with our previous study [24] is adopted, the aluminum powder with a nominal particle size of 20 μm , which is purchased from Shanghai ST-nano science and technology Co., Ltd. The results of laser particle size analyses in the sample are shown in Fig. 1. The mean diameter of the powder is approximately 20 μm . The natural bulk density of the powder sample is 1320 kg/m³.

The powder-feeding experimental system constructed in this paper is shown in Fig. 2, which mainly contains an air source, a powder-feeding device, a back-pressure simulator, and a control and measurement system. A representative gas-driven piston-type powder-feeding device is designed and implemented, Fig. 3 shows its detail technical drawing. Compared with the electric motor driving method in previous studies, the piston of the feeding device in Fig. 3 is driven by high pressure gas, which provides a convenience to monitor the operating condition of the powder feeding process, for the compressible gas is more sensitive to the change of piston motion than the rigidly connected electric motor. The powder storage box can be divided into two parts by the piston, an actuation chamber behind the piston, and a fluidization chamber near the outlet. The actuation gas and fluidization gas are both air, and the gas supplies are controlled by switching the solenoid valves. During the feeding process, the powder near the outlet of the storage box is picked up by fluidization gas and enters the delivery pipeline, while the powder near the piston is pushed forward by the piston under the action of the actuation gas. When the pressure difference between the actuation chamber and fluidization chamber is equal to the resistance required to move the piston, the piston begins to move uniformly. This creates a continuous powder supply. Finally, a pneumatic valve and a minimum flow area device are installed at the outlet of the powder storage box to control the opening and closing of the outlet and adjust its throttling area, Fig. 4 shows the throttle channels (minimum flow area device) used in this study. During the experiment, the pressure in both the actuation chamber and the fluidization chamber are recorded in real time.

Further, a back-pressure simulator is used to simulate downstream pressure during powder feeding. Because a certain length of time is necessary to establish a preset pressure, the back-pressure simulator is inflated in advance. In the experiment, stable pressure in the back-pressure simulator is achieved by precisely controlling the amount of discharged gas equal to the inflow gas. When the gas-solid flow enters the back-pressure simulator, the gas flows upward through the outlet of the back-pressure simulator, and the powder sinks to the bottom under the obstruction of the filter.

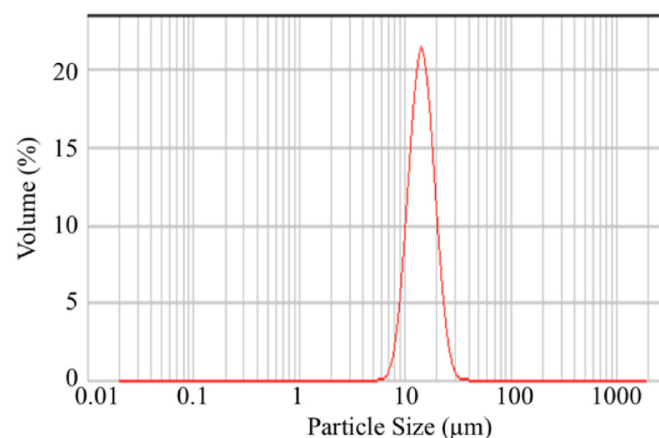
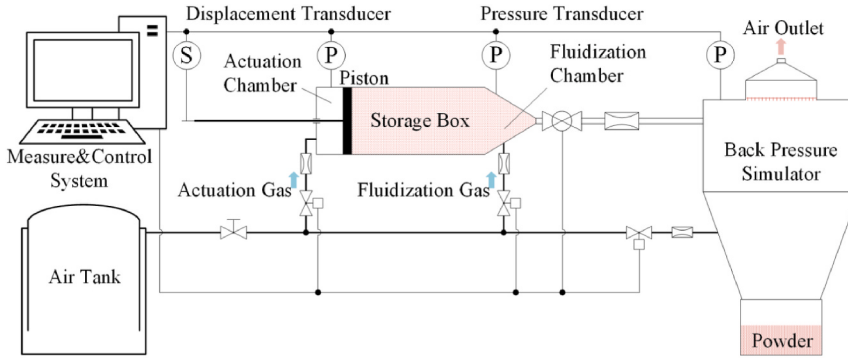
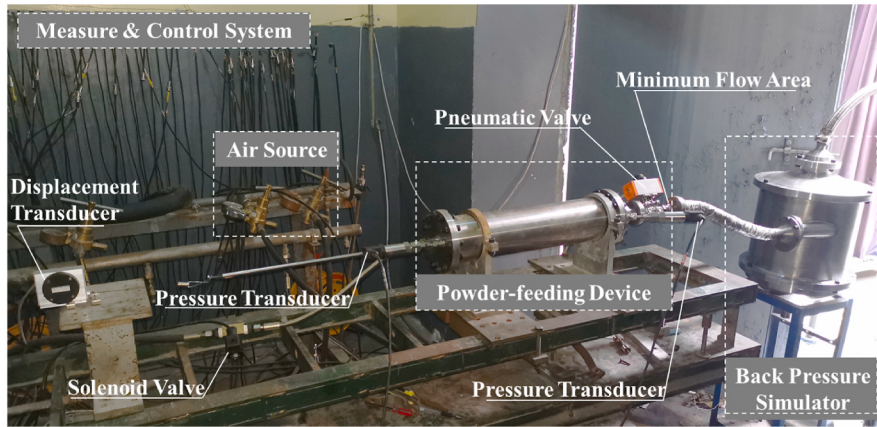


Fig. 1. Particle size distribution of aluminum powder sample.



(a) Schematic diagram of experimental system.



(b) Physical diagram of experimental system.

Fig. 2. Powder feeding experimental system.

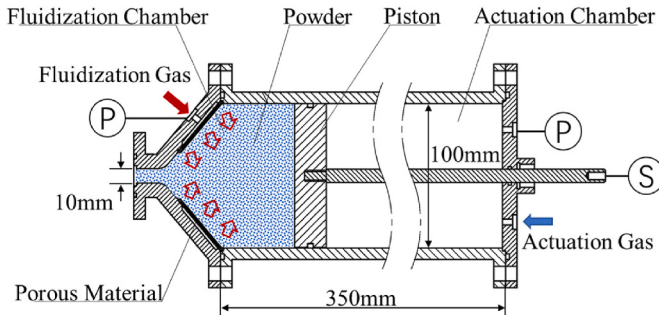


Fig. 3. Powder feeding device.

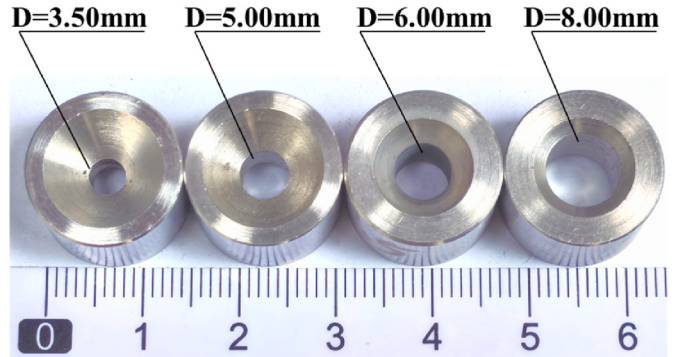


Fig. 4. The throttle channels.

2.2. Data analyses

The average mass flow rate of powder is calculated by:

$$\bar{m} = \frac{m_t - m_0}{t_t - t_0} \quad (1)$$

where \bar{m} is the average mass flow rate and m_t , m_0 , t_t , and t_0 are the mass and the corresponding moments. The mass flow rate for the transient powder mass flow rate $\dot{m}(t)$ can be obtained by:

$$\dot{m}(t) = \rho A_{\text{Piston}} v(t) = \rho A_{\text{Piston}} \frac{dS}{dt} \quad (2)$$

where ρ is powder bulk density, A_{Piston} is cross-sectional area of the piston, and v is the moving speed of the piston, which can be obtained by differentiating displacement S of the piston with respect to time t . When the piston pushes the powder to the outlet of the storage box, the bulk density ρ always changes after compression. The powder-compaction equation is often used to quantitatively describe the relationship between the powder bulk density and pressure. One of the most widely used and accurate powder compaction equations, drawn from Ref. [33], can be expressed as:

$$C = \frac{V_0 - V}{V_0} = \frac{abP}{1 + bP} \quad (3)$$

where C is the volume compression ratio of the powder, V_0 is the initial volume, V is the volume under pressure, and a and b are constant. Substituting for $m = \rho V$, the expression for powder bulk density under pressure P is obtained:

$$\rho = \left(\frac{abP}{1 + bP} + 1 \right) \rho_0 \quad (4)$$

ρ_0 is the initial powder bulk density; the value measured in this study is 1320 kg/m³. At the same time, by measuring bulk density under different pressures, a and b can be calculated. The values obtained for a and b are 0.2591 and 14.8901. Then the transient powder mass flow rate in equation (2) can be solved.

2.3. Experimental conditions

It is important for the powder-feeding system to resist the pressure disturbance caused by the downstream combustion chamber [34]. As with a pure gas flow, injection stability is strongly affected by the pressure drop between the powder feeding device and the downstream chamber. As the pressure drops, a choking phenomenon occurs at a certain pressure ratio [24,35–37] (operating pressure to downstream pressure), and flow speed in the minimum flow area reaches the speed of sound. Under these conditions, disturbances in downstream flow do not affect the state of the upstream flow. As a result, the powder-feeding system obtains the highest stability. Thus, to ensure that the investigation is carried out under the choking condition, operating parameters for all experimental conditions are set to 0.4 MPa for back pressure and 1.0 MPa for fluidization chamber pressure, which satisfies the critical pressure ratio established in the literature [24].

To obtain the powder-feeding characteristics under different gas-solid ratios, the experimental conditions are obtained by adjusting the powder mass flow rate and fluidization gas mass flow rate. The powder mass flow rate is adjusted by changing the actuation gas mass flow rate. Furthermore, because different structural features also lead to changes in the feeding characteristics, experiments are conducted under different minimum flow areas. The detailed experimental parameters for each condition are presented in Table 1. Group A is intended to obtain the influence of the actuation of the gas mass flow rate on the powder feeding characteristics, while that of Group B is to obtain the influence of the fluidization of the gas mass flow rate. Group C and Group D are the tests at minimum flow area of 36.00 mm² and 64.00 mm². Since the influence of mass flow rate of fluidization gas and powder on feeding characteristics can be obtained through Group A and Group B, only

Table 1

Experimental parameters of mass flow rate of actuation gas and fluidization gas, minimum flow area, working pressure, and back pressure. Note: The operating pressure and back pressure for all of the tests are 1 MPa and 0.4 MPa, respectively.

Group	Test number	\dot{m} of actuation gas, g/s	\dot{m} of fluidization gas, g/s	Minimum flow area, mm ²
A	1	1.2	5.0	12.25
	2	1.5		
	3	1.8		
	4	2.2		
	5	2.8		
B	6	4.0	3.0	25.00
	7		4.3	
	8		5.6	
	9		8.6	
	10		11.3	
C	11	5.4	11.0	36.00
D	12	8.1	15.0	64.00

working parameters for the stable conditions in Group C and Group D are given here, Test 11 and Test 12. Comparing the experimental results for all Groups, the operating characteristics of the powder-feeding system for different conditions of structural features can be obtained.

3. Results and discussion

3.1. Macroscopic operating characteristics of the powder-feeding system

3.1.1. Operation under different gas-solid ratios

3.1.1.1. Influence of actuation gas mass flow rate. The experimental results for Group A are shown in Fig. 5. In Tests 1 and 2 and Fig. 5(a) and (b), the pressure curves of both the actuation chamber and the fluidization chamber continue to decrease during powder feeding. Because the amount of actuation gas in the two tests are lower than in other tests, the moving speed of the piston in these two tests is consequently slower. As a result, the mass flow rate of the powder is decreased, and the fluidization gas flowing out of the powder storage box increases under the same minimum flow area. Under this circumstance, more gas flows out of the storage box than flows in, leading to a continuous decrease in fluidization pressure, which accelerates the speed of the piston. At this moment, the amount of actuation gas is insufficient to fill the excess volume in the actuation chamber left by the more rapidly moving piston in a timely fashion, finally resulting in a decreased actuation pressure. As the amount of actuation gas increases in Test 3, the pressures in the two chambers basically maintain their initial values. Under this condition, gas flowing out of the storage box is approximately equal to that flowing in, ensuring a balanced pressure on both sides of the piston. The actuation gas fills the chamber created by the piston's movement. However, there is an obvious low-frequency oscillation in the pressure curves of Test 3.

Continuing to increase actuation gas mass flow rate in Test 4 and Test 5, a slight increase in fluidization pressure and a rapid increase in actuation pressure can be seen. This is because the powder mass flow rate exceeds the limitations of the minimum flow area at the outlet of the powder storage box. The extra powder that goes beyond the maximum value cannot be taken out in a timely fashion, and under this circumstance, the gas flowing out of storage box is less than that flowing in. As a result, the fluidization pressure increases, and the extra actuation gas beyond the design value is only used to increase the actuation pressure. The powder in Test 4 and Test 5 might be more compacted than that in Test 1 and Test 2 because the pressure difference between the two sides of piston is significantly increased.

3.1.1.2. Influence of fluidization gas mass flow rate. The experimental curves for Group B are shown in Fig. 6. In Test 6, the mass flow rate of the fluidization gas is 3.0 g/s. Due to the insufficient amount of fluidization gas, the existing gas inside the fluidization chamber needs to carry the powder out. As a result, the pressure drop in the fluidization chamber is obvious. In Test 7, when the fluidization gas increases to 4.3 g/s, the pressure in the fluidization chamber shows a slight downward trend. When it is further increased to 5.6 g/s, Test 8, there is little change in the experimental results compared to Test 7. As can be seen from the curves of Test 9 and Test 10, the pressure in the fluidization chamber has a slight upward trend, indicating that the actual amount of gas flowing out of the storage box is less than the gas entering the fluidization chamber. Moreover, the actuation pressure curves in Group B show a similar variation rule as Group A.

3.1.2. Average powder mass flow rate

The experimental curves of the stable conditions, Test 11 and Test 12, for Group C and Group D are shown in Fig. 7. Average powder mass flow rates are 417 g/s and 716 g/s, respectively. The actuation and fluidization pressure curves show a similar variation rule as Group A and

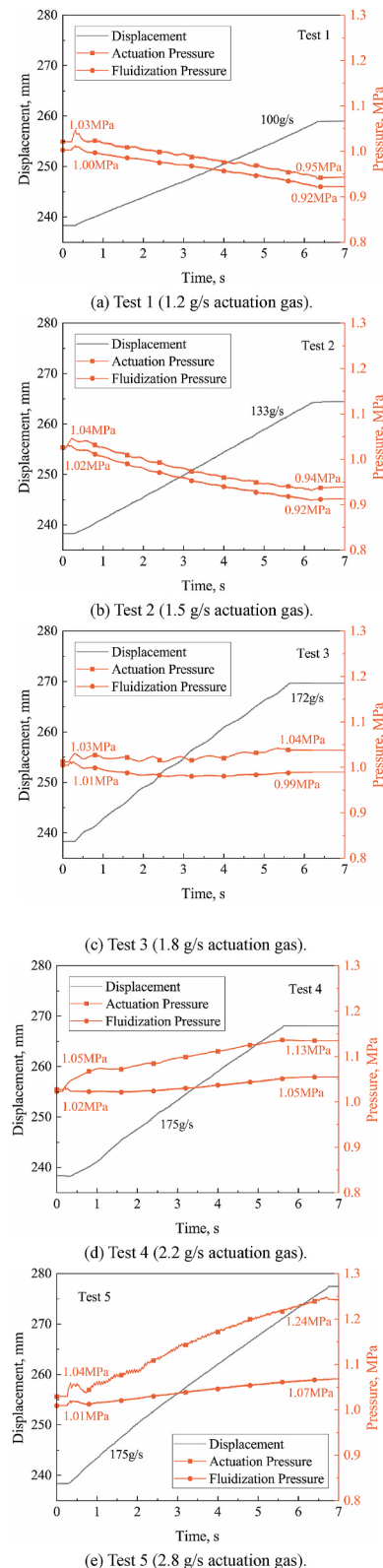


Fig. 5. Experimental results of Group A (5 g/s fluidization gas, 12.25 mm² minimum flow area).

Group B. The obtained average powder mass flow rate and corresponding gas-solid mass ratio are plotted in Fig. 8. Compared to Group B, the range of variation in the gas-solid ratio covered by Group A is relatively limited, so the experimental results show only the rule that the average powder mass flow rate decreases with an increase in the gas-

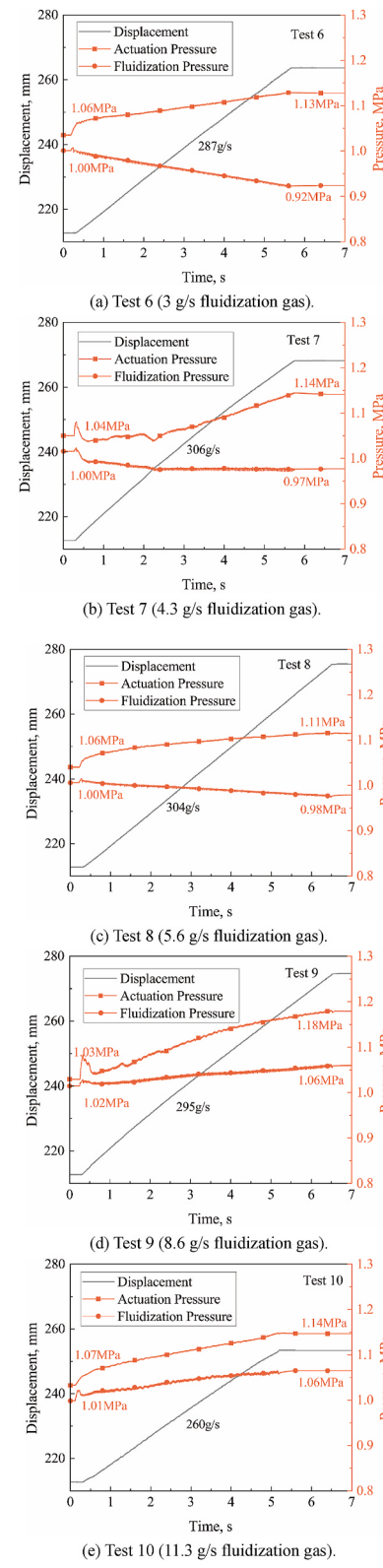


Fig. 6. Experimental results of Group B (4 g/s actuation gas, 25.00 mm² minimum flow area).

solid ratio. For Group B, the average mass flow rate of powder increases with an increase in the fluidization gas; however, when the amount of gas fluidization reaches a certain level, the average mass flow rate of powder does not increase but rather decreases, as shown in Test 7. When comparing the results of Group A and Group B, the actuation

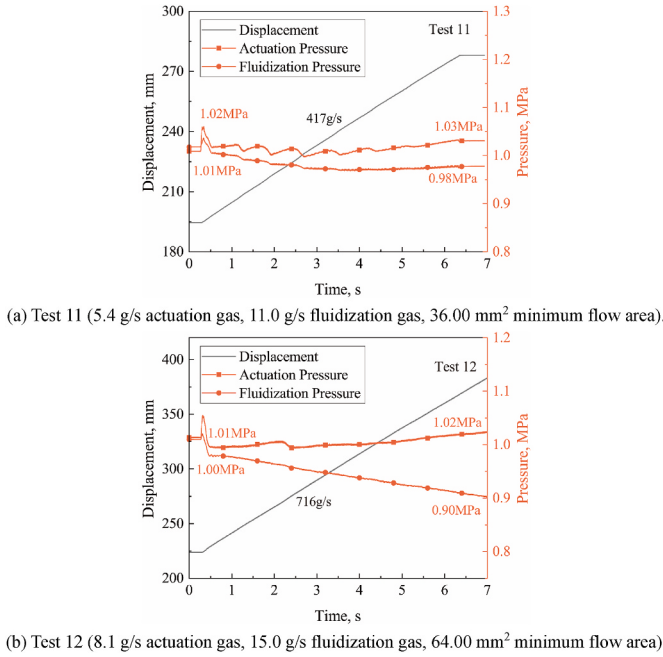


Fig. 7. Experimental results of Group C and Group D.

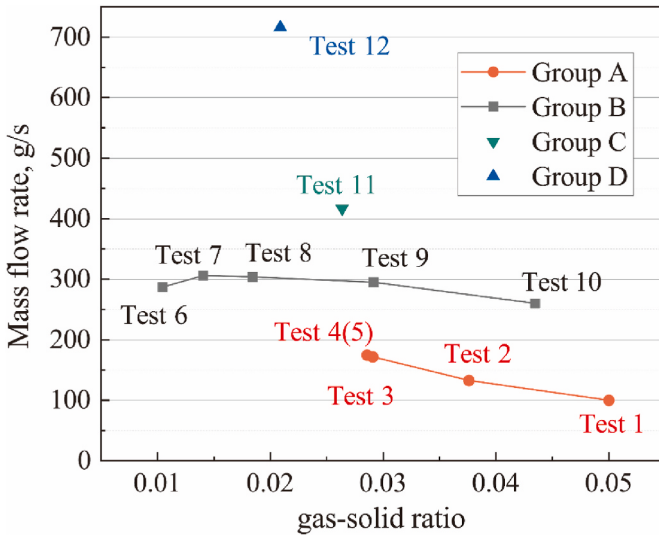


Fig. 8. Experimental results from the tests.

gas exhibits a larger influence on average powder mass flow rate. The maximum and minimum average powder mass flow rates are 175 g/s (Test 5) and 100 g/s (Test 1) for Group A, with a variation range of 75%, and 306 g/s (Test 5) and 260 g/s (Test 1) for Group B, with a variation range of 18%. This is largely because the actuation gas acts directly on the piston's movement.

The above analyses show that the operating process of the powder-feeding system is relatively complex. Whether the flow state of powder is statistically steady can be identified according to the fluidization chamber pressure variation range. From a fundamental viewpoint, the energy is input into the fluidization chamber by the inflow gas, which is dissipated by gas-particle, particle-particle, and particle-wall interactions. Finally, when the gas-solid ratio matches the main structural parameters well, the system maintains a statistically steady state but one that is far from equilibrium. As seen in Test 3 in Group A and Test 7 in Group B, the variation range of the fluidization chamber pressure is relatively small. Analyzing the process of the piston pushing the powder

forward, it can be seen that all of the powder in the storage box is not pushed forward at the same time when the piston begins to move. Rather, the powder closer to the piston is pushed first, then the powder further from the piston is gradually promoted. As this unfolds, the powder experiences a certain compression due to the gaps among the particles. At the same time, the stable pressure difference between the fluidization pressure and the actuation pressure does not lead to the equilibrium of the system but indicates that the powder is not compacted under this circumstance, such as in Test 1, Test 2, and Test 10. Moreover, comparing the the.

3.2. Analyses of transient powder mass flow rate

3.2.1. Compression pressure in powder feeding

When the piston pushes the powder to the outlet of the storage box, the bulk density of powder changes after compression. According to equation (2), analysis of compression pressure is necessary for powder bulk density calculation. Moreover, analysis of compression pressure is helpful for judging the characteristics of the motion of the piston. The compression pressure can be computed from the pressure differences between the actuation chamber and fluidization chamber. Figs. 9 and 10 show the compression pressure for each test of Group A and Group B, respectively.

The compression pressure curves show an obvious high-frequency oscillation, which is largely caused by the pressure disturbance in the fluidization chamber induced by the high uncertainty of the bubbling and/or clustering structures in the gas-solid flow. In Fig. 9, the compression pressure of Test 1 and Test 2 is maintained in a stable state, which indicates that the powder in the storage box under Test 1 and Test 2 rapidly reached a stable state during the feeding process. The downward trend of the pressure curves in Fig. 5(a) and (b) implies that the powder is in a slack state throughout the entire feeding process. The compression pressure of Test 3 to Test 5 gradually increased, indicating that the powder did not reach a stable state within the given experimental time. The process of piston gradually promoting the whole powder, and the process of powder compression will both eventually lead to the increasing of compression pressure. Moreover, compression pressure increases with a decrease in the gas-solid ratio and an increase in the actuation gas mass flow rate.

For Group B, the compression pressure curve of Test 7 shows a different variation rule compared to other curves in Fig. 10, which is mainly caused by the movement condition change of the piston.

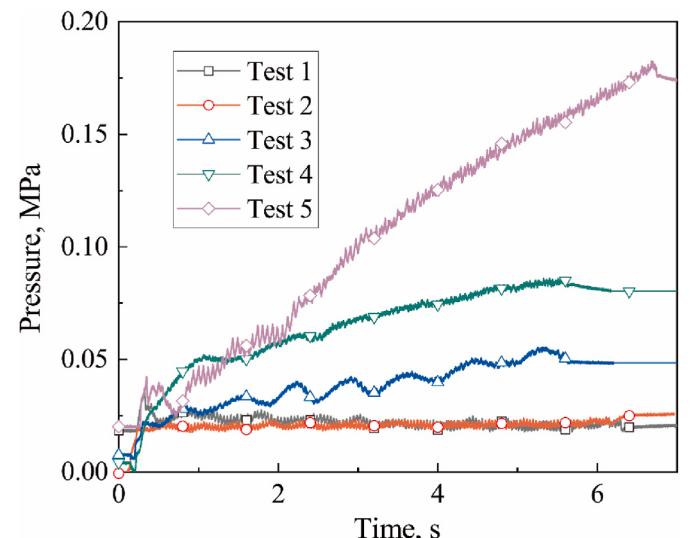


Fig. 9. Pressure difference behind and before the piston with respect to time of Group A.

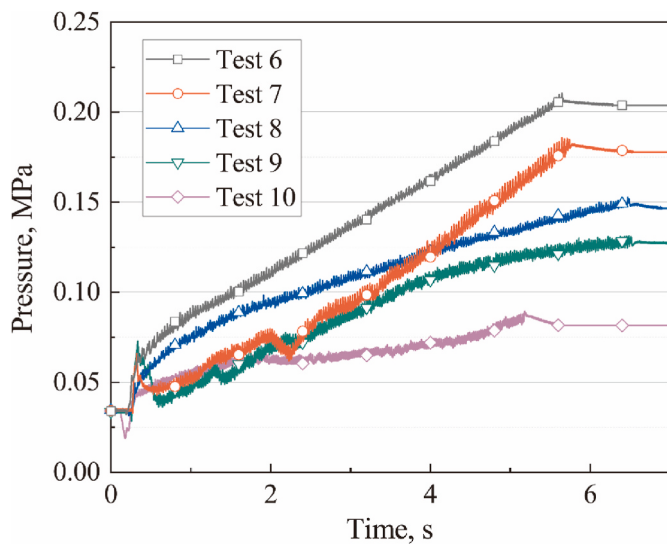


Fig. 10. Pressure difference behind and before the piston with respect to time of Group B.

However, with the exception of this irregular curve, the other curves present a similar rule to that shown in Fig. 9. The pressure curves of Test 6 to Test 10 gradually decrease with increases in both the gas-solid ratio and the fluidization of the gas mass flow rate. However, within the time of a given experiment, Test 6 to Test 10 did not reach a stable state.

3.2.2. Transient powder mass flow rate

Based on the above analyses of the compression pressure, Figs. 11 and 12 show the results of transient powder mass flow rate calculated by formula (2). The corresponding average, maximum, and minimum mass flow rates are also given.

For both Group A and Group B, the transient mass flow rate curves show obvious high-frequency and low-frequency oscillations. Combined with the compression pressure in Figs. 9 and 10, a high correlation can be found between transient mass flow rate and compression pressure, such as the obvious low-frequency oscillation in Test 3, for which the relative mass flow rate deviation reaches -42% to $+76\%$. The experimental curves for Test 1 and Test 2 are relatively smooth and steady, and the relative deviations for mass flow rate are -20% to $+30\%$ and -16% to $+26\%$, respectively. The curve in Test 5 shows a trend of gradual decrease during the initial seconds, $t = 0\text{ s}$ to $t = 3\text{ s}$, which is mainly caused by the progressively slower piston speed, as shown in Fig. 11, and the increase in compression pressure.

For Group B, the most smooth and steady result is Test 8, and the relative deviation of powder mass flow rate is -15% to $+8\%$. The experimental curves for Test 6, Test 7, Test 9, and Test 10 all show a trend of gradual decrease, and combined with actuation pressure curves given in Fig. 6, the actuation pressure of these four tests all exhibit an obviously greater uptrend than Test 8. Comparing the results for Group A with those of Group B, the curves of Group B appear more stable, largely because the operating conditions of Group B are closer to the optimum parameters matching the structure features and operating range of the powder-feeding system.

3.3. Analyses of pressure oscillation characteristics

The macroscopic operating characteristics of the powder-feeding system and the transient mass flow rate show obvious oscillations. Hence, changes in piston movement and the powder flow state in the fluidization chamber lead to dramatic pressure-signal changes in the actuation chamber and the fluidization chamber, respectively [38]. Thus, to obtain the oscillation characteristics of piston movement and

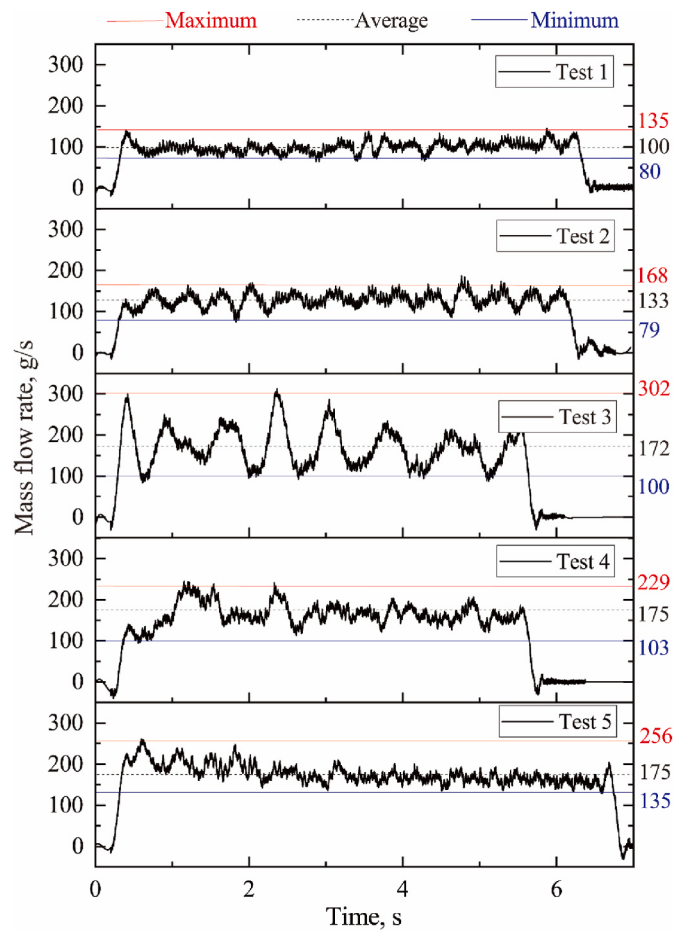


Fig. 11. Powder transient mass flow rate of Group A.

the powder flow state, the pressure signals in the actuation chamber and fluidization chamber are analyzed using the fast Fourier transform method. Frequency domain curves of the tests are shown in Figs. 13 and 14. The pressures in both chambers show obvious oscillations. For the FFT results of the actuation pressure, there exist obvious low-frequency oscillations and high-frequency oscillations. The frequencies of notable low-frequency oscillations are mainly 1–3 Hz for both Group A and Group B, while those of notable high-frequency oscillations are 20–30 Hz for Group A and 30–45 Hz for Group B. These all coincide well with the corresponding transient mass flow curves in Figs. 11 and 12.

Because the most obvious difference among the tests for Group A is the actuation gas mass flow rate, the FFT results of actuation pressure exhibit obvious distinctions, while those of the fluidization pressure are basically similar to each other. For Group B, the actuation chamber features mainly low-frequency oscillations, while in the fluidization chamber high-frequency oscillations are seen. The high-frequency oscillation shows an obvious law in that the frequency at the maximum amplitude increases with increasing fluidization gas. It is easy to see that this high-frequency oscillation in fluidization chamber is caused by the complex mesoscale bubbling and/or clustering structures during the gas-solid transport process. In Group A, the mass flow rates of powder are smaller, there is little powder clogged at the throttle channel, as a result, almost no high-frequency oscillation is found in fluidization pressure. However, in Group B, with increasing powder mass flow rate, powder is easily clogged at the throttle channel. When fluidization gas is increased, the interaction between powder and fluidization gas is stronger. Therefore, it takes a shorter time to blow the clogged powder out of the throttle channel, so the oscillation frequency is larger. It can be inferred that the oscillation may be an inherent defect of the existing powder supply device, which will have a noticeable effect on

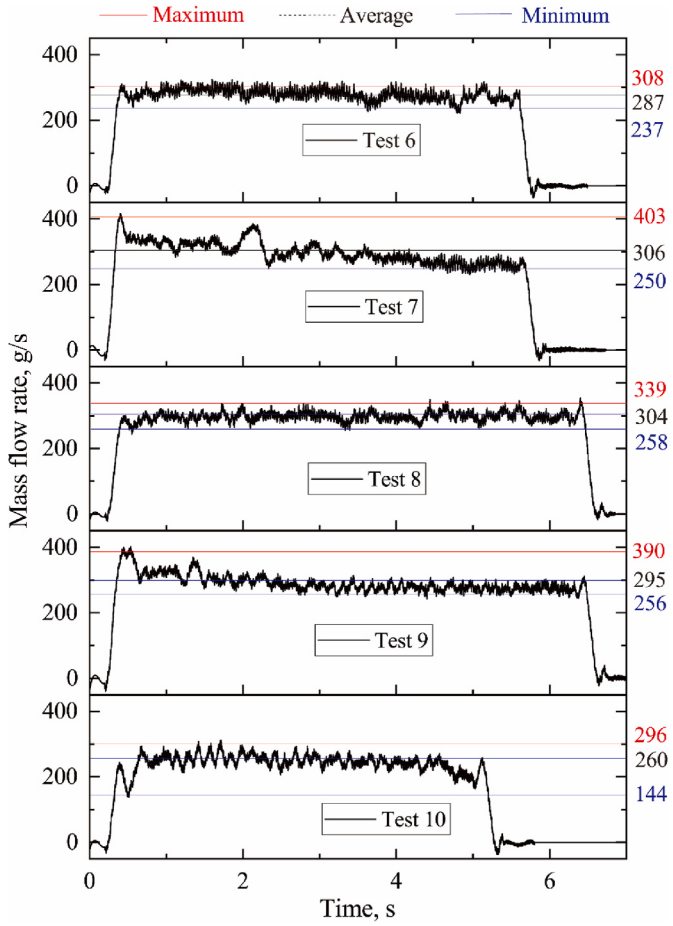


Fig. 12. Powder transient mass flow rate of Group B.

the chamber pressure. To minimize or suppress these oscillations, it is necessary to carry out more targeted and microscopic investigations on the relationships between the characteristics of the gas-solid flow structure and its oscillations.

3.4. Quantitative analysis on stable powder-feeding

According to analysis above, the mass flow rate of powder, fluidization gas, and the minimum flow area of the throttle channel all play an important role in powder feeding process. The relationship between above parameters during solid-gas two phase flow under choking condition can be described by the following equation [14].

$$\dot{m} = \frac{P_0 A_{min}}{\sqrt{R_m T_0}} \sqrt{\gamma_m} \left[\frac{2}{\gamma_m + 1} \right]^{\frac{\gamma_m + 1}{2(\gamma_m - 1)}} \quad (5)$$

here P_0 is the stagnation pressure of the two-phase flow in fluidization chamber, A_{min} is the minimum cross-sectional area of the delivery pipeline, R_m is the two-phase mixture constant, T_0 is the stagnation temperature, and γ_m is the specific heat ratio of gas solid mixture. It can be seen from equation (5) that under a given stagnation pressure, the powder mass flow rate is mainly decided by the minimum area of the throttle channel, that is

$$\dot{m} \propto A_{min} \quad (6)$$

Fig. 15 illustrates the relationship between A_{min} and \dot{m} measured in this paper under stable operation state. The corresponding solid-gas mass ratios are also plotted at the same time. It is observed that a high linear tendency between A_{min} and \dot{m} , with slope valued 10.50, R square valued 0.9997. On the other hand, it is evident that the solid-gas mass

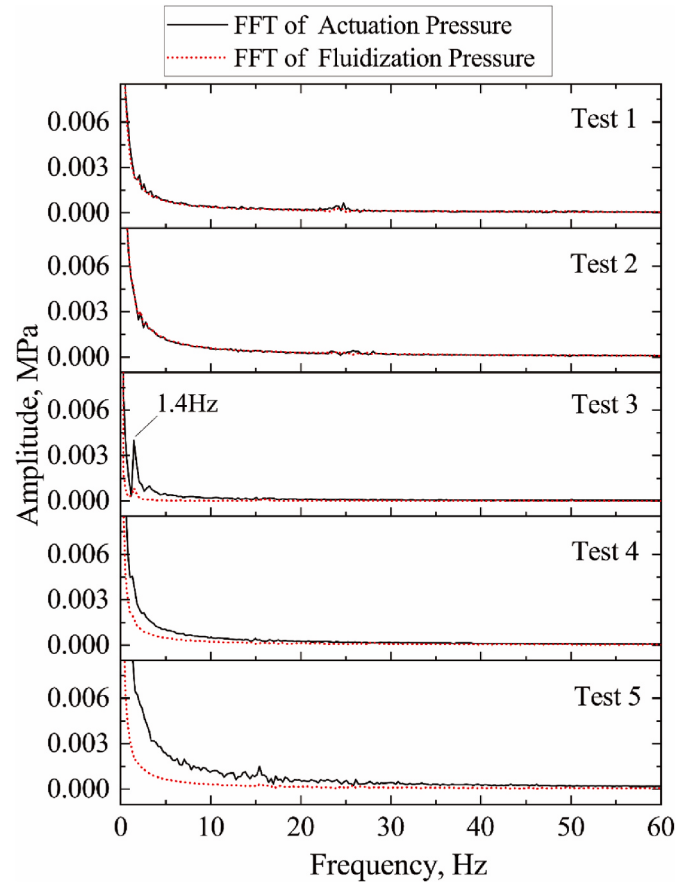


Fig. 13. FFT analysis results of actuation and fluidization pressure for Group A.

ratio to maintain a stable operation of the powder feeding system is valued in range of 34.4–54.6. Which provides a quantitative description for powder mass flow rate prediction in powder feeding process under choking condition, the most important parameter in guiding engineering design. According to this criterion, the two most critical parameters in powder-feeding system design can be obtained, that is the solid-gas mass ratio to maintain a stable operation and the minimum area of throttle channel. The design procedure can be elaborated as follows: firstly, the solid-gas mass ratio to maintain a stable operation is determined in range of 34.4–54.6, then, according to the requirement of powder mass flow rate, an appropriate throttle channel area is obtained by the correlation.”

4. Conclusion

The operating characteristics of a classic piston-driven powder-feeding system were investigated experimentally under different gas-solid ratios. By adjusting the actuation gas and fluidization gas mass flow rate, the powder-feeding mass flow rate and pressure oscillation characteristics of the powder-feeding system under different parameters were obtained. The main conclusions are summarized below:

- (1) The stable operating process of the powder-feeding system was obtained through a good match of fluidization gas and actuation gas mass flow rate, as well as the minimum flow area. The average mass flow rate of powder increases with an increase in the actuation gas, but when that gas reaches a certain level, it does not increase significantly.
- (2) As the gas-solid ratio decreases, powder compression pressure increases. As the operating conditions reach an optimum, the powder-feeding process becomes more stable. The deviation in

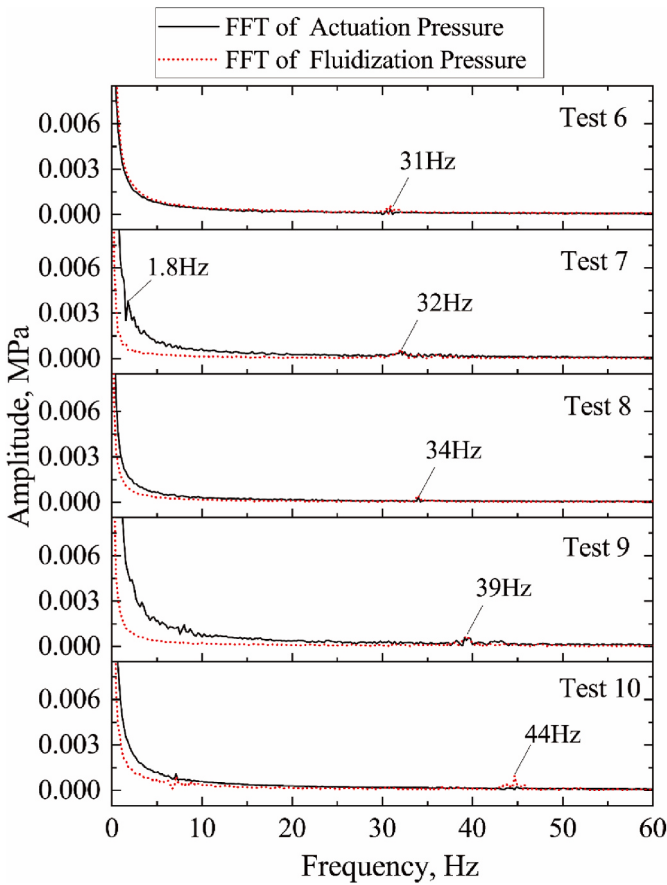


Fig. 14. FFT analysis results of actuation and fluidization pressure for Group B.

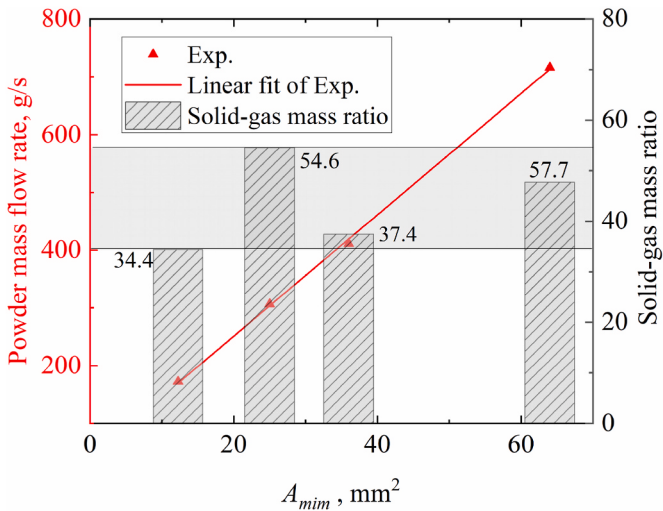


Fig. 15. Relationship between A_{min} and the powder mass flow rate, and the corresponding solid-gas mass ratio for stable feeding process.

the relative powder mass flow rate for the most smooth and steady test is -15% to $+8\%$.

- (3) Because of the high uncertainty of the gas-solid flow structures under different gas-solid ratios, there are certain obvious low-frequency oscillations and high-frequency oscillations during the powder-feeding process. The frequencies of low-frequency oscillations are mainly 1–3 Hz for both Group A and Group B,

while those of high-frequency oscillations are 20–30 Hz for Group A and 30–45 Hz for Group B.

- (4) A high linear tendency between powder mass flow rate and the minimum throttle channel area is observed from the experiment, with slope valued 10.50, R square valued 0.9997. The solid-gas mass ratio to maintain a stable powder feeding is approximately valued in range of 34.4–54.6 under different throttle channel areas.

Declaration of competing interest

This revised manuscript has not been published or presented elsewhere in part or in entirety and is not under consideration by another journal. We have read and understood your journal's policies, and we believe that neither the manuscript nor the study violates any of these. There are no conflicts of interest to declare.

Acknowledgments

This work was supported by the National Natural Science Foundation of China [No. 52006169] and the 'Open, cooperate and innovate fund' of Xi'an Modern Chemistry Research Institute [SYJJ38].

References

- [1] H. Loftus, L. Montanino, R. Bryndle, Powder rocket feasibility evaluation[C], in: 8th Joint Propulsion Specialist Conference, 1972.
- [2] Y. Li, C. Hu, Z. Deng, et al., Experimental study on multiple-pulse performance characteristics of ammonium perchlorate/aluminum powder rocket motor[J], Acta Astronaut. 133 (2017) 455–466.
- [3] C. Li, C. Hu, X. Xin, et al., Experimental study on the operation characteristics of aluminum powder fueled ramjet[J], Acta Astronaut. 129 (2016) 74–81.
- [4] Y.J. Yang, M.G. He, Numerical study on operating characteristics of a magnesium-based fuel ramjet[J], Acta Astronaut. 79 (2012) 96–106.
- [5] S. Goroshin, A. Higgins, J. Lee, Powdered magnesium-carbon dioxide propulsion concepts for Mars missions[C], in: 35th Joint Propulsion Conference and Exhibit, 1999.
- [6] C. Li, C. Hu, X. Zhu, et al., Experimental study on the thrust modulation performance of powdered magnesium and CO₂ bipropellant engine[J], Acta Astronaut. 147 (2018) 403–411.
- [7] X. Zhu, C. Li, Y. Guo, et al., Experimental investigation on the ignition and combustion characteristics of moving micron-sized Mg particles in CO₂[J], Acta Astronaut. 169 (2020) 66–74.
- [8] C. Hu, C. Li, H. Sun, et al., A summary of powder fueled ramjet [J], J. Solid Rocket Technol. 40 (3) (2017) 269–276.
- [9] J. Wang, Continuum theory for dense gas-solid flow: a state-of-the-art review[J], Chem. Eng. Sci. 215 (2019) 115428.
- [10] H.D. Fricke, J.W. Burr, et al., Fluidized powders-A new approach to storable missile fuels[C], in: 12th JANNAF Liquid Propulsion Meeting, 1970.
- [11] T.F. Miller, A high-pressure, continuous-operation cyclone separator using a water-generated flow restriction[J], Powder Technol. 122 (1) (2002) 61–68.
- [12] T.M. Baker, T.F. Miller, Ultraviolet radiation from combustion of a dense magnesium powder flow in air[J], J. Thermophys. Heat Tran. 27 (1) (2013) 22–29.
- [13] D.F. Waters, C.P. Cadou, W.E. Eagle, Quantifying unmanned undersea vehicle range improvement enabled by aluminum-water power system[J], J. Propul. Power 29 (3) (2013) 675–685.
- [14] H. Sun, C. Hu, T. Zhang, et al., Experimental investigation on mass flow rate measurements and feeding characteristics of powder at high pressure[J], Appl. Therm. Eng. 102 (2016) 30–37.
- [15] J. Foote, R. Litchford, Powdered magnesium-carbon dioxide combustion for mars propulsion[C], in: 41st AIAA/ASME/SAE/ASEE Joint Propulsion Conference & Exhibit, 2005.
- [16] M.L. Meyer, Powdered aluminum and oxygen rocket propellants: subscale combustion experiments[R], NASA Tech. Memo. 106439 (1993).
- [17] T. Miller, J. Herr, Green rocket propulsion by reaction of Al and Mg powders and water[C], in: 40th AIAA/ASME/SAE/ASEE Joint Propulsion Conference and Exhibit, 2004.
- [18] V.I. Malinin, E.I. Kolomin, I.S. Antipin, Ignition and combustion of aluminum-air suspensions in a reactor for high-temperature synthesis of alumina powder, Combustion [J]. Explosion and Shock Waves 38 (5) (2002) 525–534.
- [19] D.A. Yagodnikov, Experimental study of combustion of a cloud of boron particles in air [J], Combust. Explos. Shock Waves 46 (4) (2010) 426–432.
- [20] A.S. Tizilov, A.G. Egorov, Limits of flame propagation in an aluminum-air mixture flow [J], Russ. J. Phys. Chem. B 7 (2) (2013) 133–136.
- [21] S. Goroshin, A. Higgins, M. Kamel, Powdered metals as fuel for hypersonic ramjets [C], in: 37th Joint Propulsion Conference and Exhibit, 2001, p. 3919.
- [22] S. Goroshin, I. Fomenko, J.H.S. Lee January, Burning velocities in fuel-rich aluminum dust clouds [J], The Combustion Institute 26 (2) (1996) 1961–1967.

- [23] Grant A. Risha, Ying Huang, Richard A. Yetter, et al., Combustion of aluminum particles with steam and liquid water [C], in: 44th AIAA Aerospace Sciences Meeting and Exhibit, 2006, p. 1154.
- [24] J. Yang, C. Hu, W. Qiang, et al., Experimental investigation on the starting and flow regulation characteristics of powder supply system for powder engines[J], *Acta Astronaut.* 180 (2021) 73–84.
- [25] J. Yang, C. Hu, X. Zhu, et al., Experiment study of characteristics of powder pneumatic filling[J], *Acta Phys. Sin.* 69 (4) (2020) 275–283.
- [26] X. Zhu, C. Hu, J. Yang, et al., Research of filling ratio and fluidization performance of dense-packing aluminum powder[J], *J. Northwest. Polytech. Univ.* 37 (1) (2019) 13–20.
- [27] H. Sun, C. Hu, X. Zhu, et al., Numerical simulation on the powder propellant pickup characteristics of feeding system at high pressure, *Acta Astronautica* 139 (2017) 85–97.
- [28] E. Rabinovich, H. Kalman, Pickup, critical and wind threshold velocities of particles[J], *Powder Technol.* 176 (1) (2007) 9–17.
- [29] H. Kalman, A. Satran, D. Meir, et al., Pickup (critical) velocity of particles[J], *Powder Technol.* 160 (2) (2005) 103–113.
- [30] D. Dasani, C. Cyrus, K. Scanlon, et al., Effect of particle and fluid properties on the pickup velocity of fine particles[J], *Powder Technol.* 196 (2) (2009) 237–240.
- [31] J. Li, J.A.M. Kuipers, Effect of pressure on gas–solid flow behavior in dense gas–fluidized beds: a discrete particle simulation study[J], *Powder Technol.* 127 (2) (2002) 173–184.
- [32] H. Sun, C. Hu, X. Zhu, et al., Experimental investigation on incipient mass flow rate of micro aluminum powder at high pressure[J], *Exp. Therm. Fluid Sci.* 83 (2017) 231–238.
- [33] K. Kawakita, K. Lutte, Some considerations on powder compression equations[J], *Powder Technol.* 4 (2) (1971) 61–68.
- [34] C. Li, C. Hu, G. Wu, et al., Investigation on effects of injection pressure drop on Al/AP powder rocket motor operation characteristics[J], *J. Propuls. Technol.* 39 (12) (2017) 2873–2880.
- [35] T. Han, A. Levy, H. Kalman, et al., Model for dilute gas–particle flow in constant-area lance with heating and friction[J], *Powder Technol.* 112 (3) (2000) 283–288.
- [36] X. Wang, Q. Li, Z. Zou, et al., Experimental study on choking phenomenon of gas–powder flow[J], *Chin. J. Process Eng.* 5 (6) (2005) 591–596.
- [37] Q. Li, M.X. Feng, Z. Zou, et al., Choking phenomenon used as an approach to measure sonic velocity of air–powder two-phase flow[J], *J. Northeast. Univ. (Nat. Sci.)* 28 (10) (2007) 1417–1420.
- [38] H. Sun, C. Hu, Y. Xu, et al., Multiscale Analysis of powder-propellant conveying stability through a nozzle [J], *J. Fluid Eng.* 141 (10) (2019) 101302.